

## Supplementary information

### Dual client binding sites in the ATP-independent chaperone SurA

Bob Schiffrin<sup>1\*</sup>, Joel A. Crossley<sup>1\*</sup>, Martin Walko<sup>1,2</sup>, Jonathan M. Machin<sup>1</sup>, G. Nasir Khan<sup>1</sup>,  
Iain W. Manfield<sup>1</sup>, Andrew J. Wilson<sup>2,3</sup>, David J. Brockwell<sup>1</sup>, Tomas Fessl<sup>4</sup>, Antonio N.  
Calabrese<sup>1</sup>, Sheena E. Radford<sup>1#</sup>, Anastasia Zhuravleva<sup>1#</sup>

<sup>1</sup>Astbury Centre for Structural Molecular Biology, School of Molecular and Cellular Biology,  
Faculty of Biological Sciences, University of Leeds, Leeds LS2 9JT

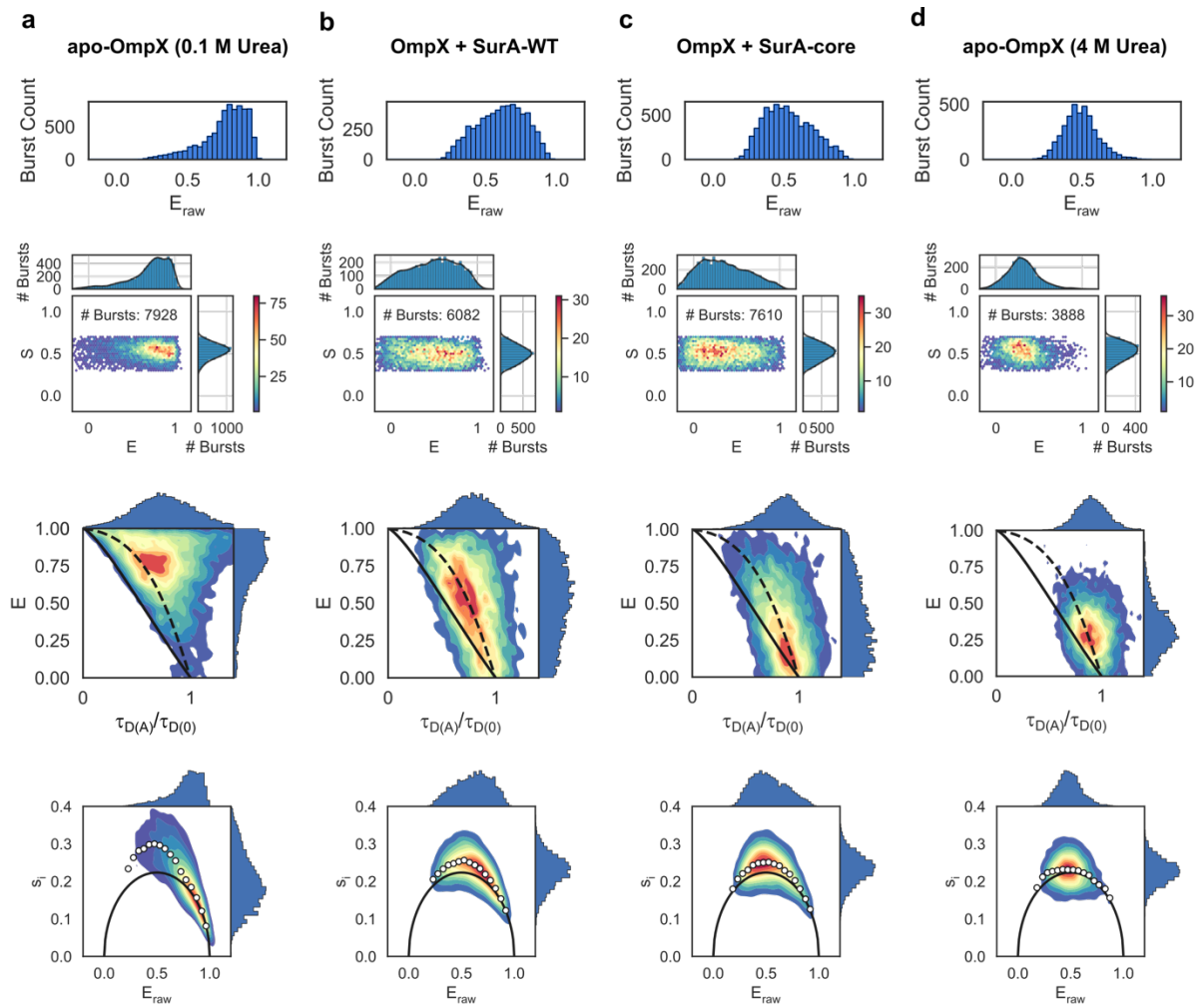
<sup>2</sup>Astbury Centre for Structural Molecular Biology, School of Chemistry, University of Leeds,  
Leeds LS2 9JT

<sup>3</sup>Current address: School of Chemistry, University of Birmingham, Edgbaston, Birmingham,  
B15 2TT, UK

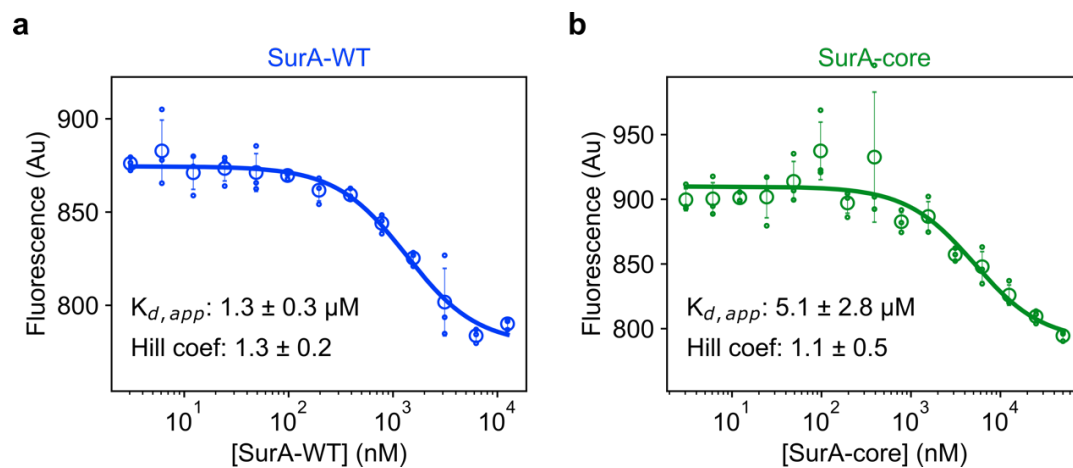
<sup>4</sup>Faculty of Science, University of South Bohemia, Branišovská 1760, 370 05 České  
Budějovice, Czech Republic

\*Equal contribution

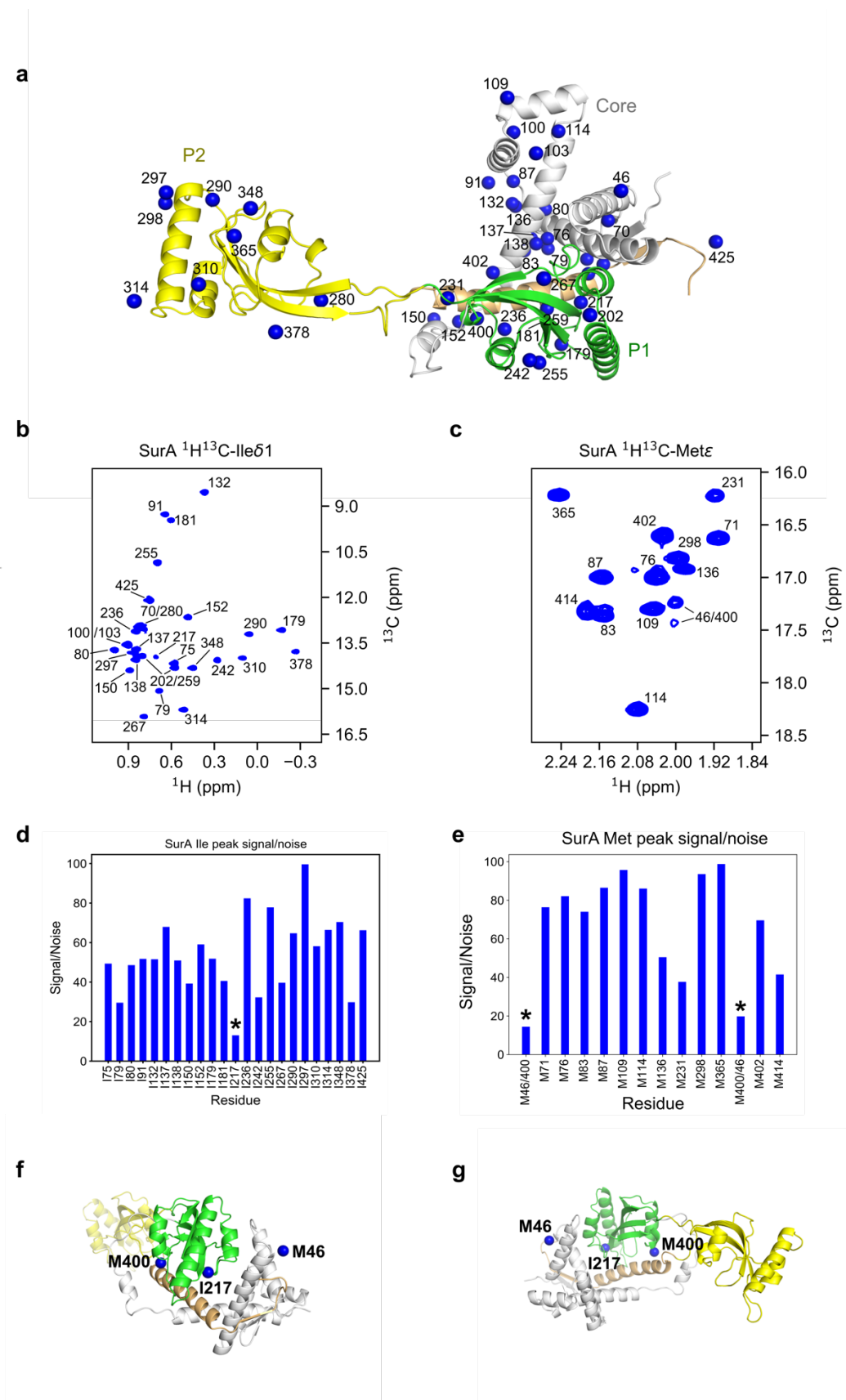
#To whom correspondence should be addressed: [s.e.radford@leeds.ac.uk](mailto:s.e.radford@leeds.ac.uk) and  
[a.zhuravleva@leeds.ac.uk](mailto:a.zhuravleva@leeds.ac.uk)



**Supplementary Fig. 1.** smFRET data for labelled OmpX in the presence or absence of SurA variants. Data are shown for (a) apo-OmpX (0.1 M urea), (b) OmpX + SurA-WT, (c) OmpX + SurA-core, and (d) apo-OmpX (4 M urea). The top row shows the uncorrected FRET efficiency histograms ( $E_{raw}$ ) of filtered FRET bursts. The second row shows corrected FRET efficiency ( $E$ ) vs stoichiometry ( $S$ ) for the filtered FRET bursts. The third row shows plots of  $E$  versus normalised fluorescence donor lifetime ( $\tau_{D(A)}/\tau_{D(0)}$ ) (Methods). The solid black line represents the correlation between these two values expected for a static ( $\leq$  ms timescale) FRET species. FRET populations which deviate to the right from this line exhibit dynamics. The dashed black line represents the expected correlation between  $E$  and  $\tau_{D(A)}/\tau_{D(0)}$  for a rapidly interconverting Gaussian chain. The fourth row shows Burst Variance Analysis (BVA) where  $E_{raw}$  is plotted vs the standard deviation in the burst ( $s_i$ ). The solid black line represents the expected standard deviation for a static (ms timescale) FRET population. The white circles show the mean  $s_i$  for bin widths of 0.05 of  $E_{raw}$ . Source data are provided as a Source Data file.

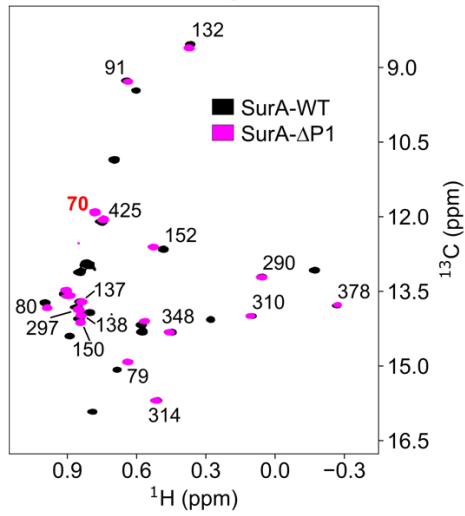
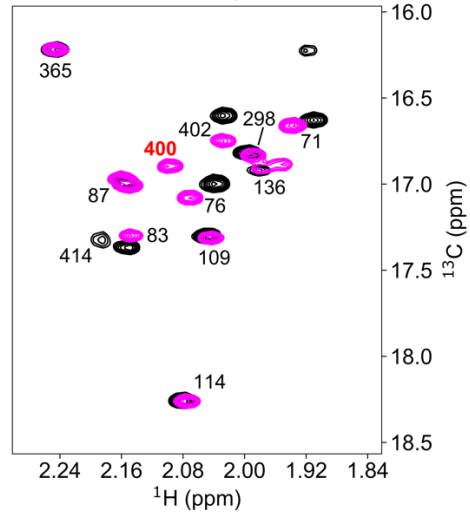
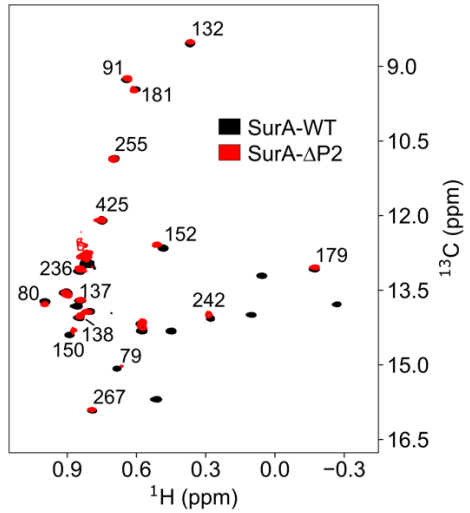
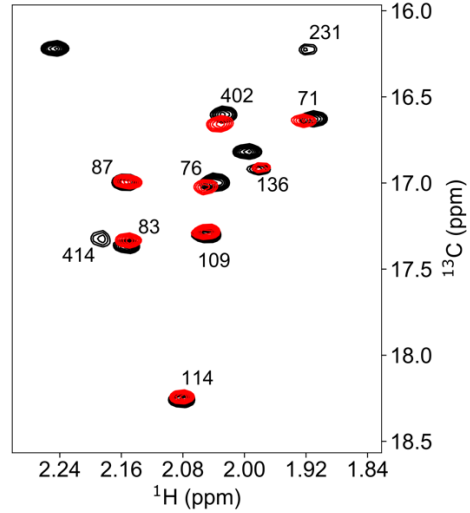
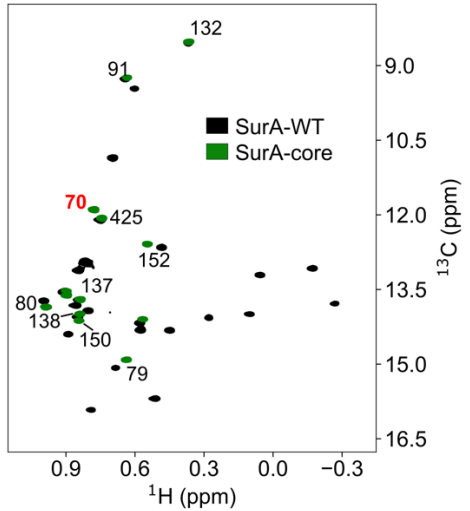
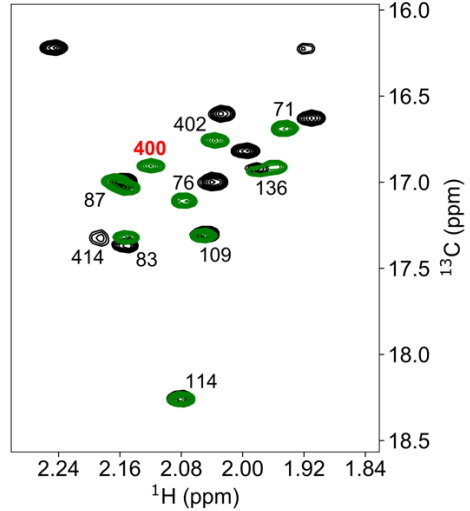


**Supplementary Fig. 2.** Microscale thermophoresis (MST) data for binding of OmpX to (a) SurA-WT, and (b) SurA-core. Samples contained 100 nM Alexa Fluor 488-labelled OmpX (Methods), SurA-WT (3 nM-50  $\mu\text{M}$ ), 0.8 M urea, 20 mM Tris-HCl, pH 8, at 25  $^{\circ}\text{C}$ . Three independent replicates were performed and averaged prior to fitting. The mean for each SurA-WT or SurA-core concentration is shown as open circles and the individual values for each replicate are shown as dots. The error bars represent the standard deviation between replicates. Data were fitted to a Hill binding equation (Methods). Source data are provided as a Source Data file.

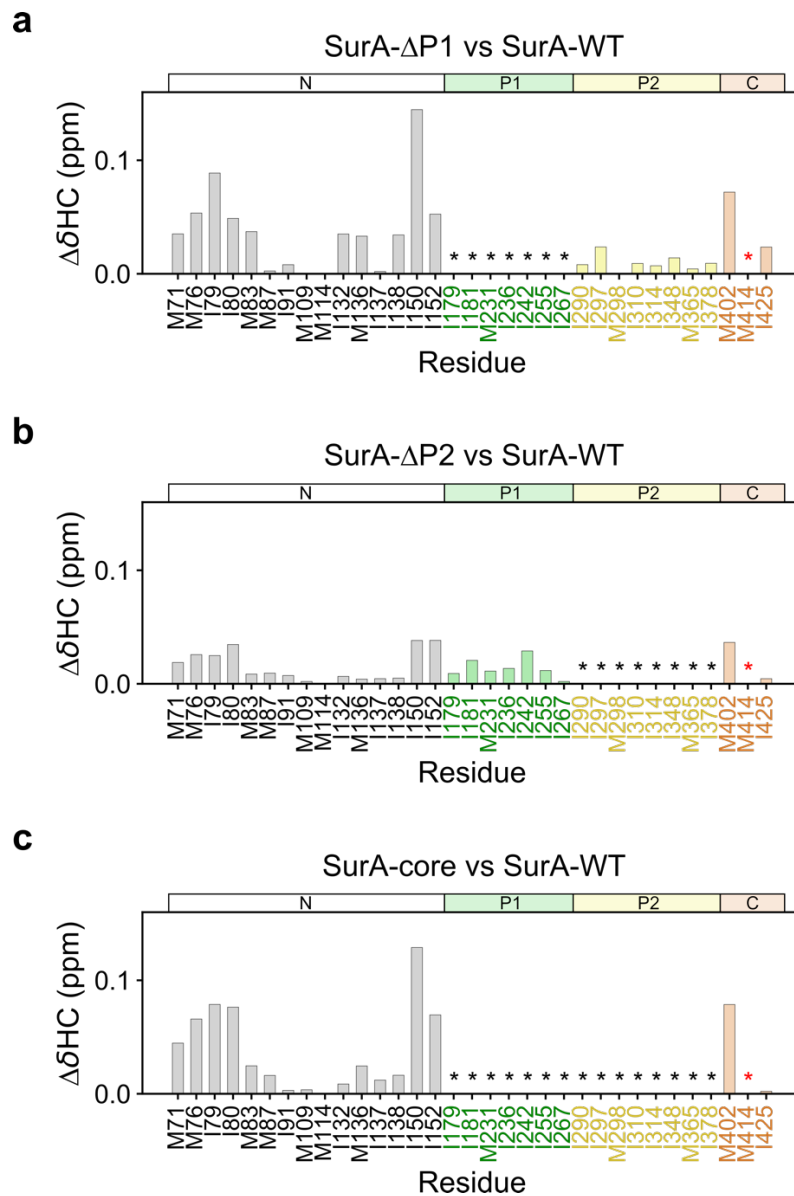


**Supplementary Fig. 3.** Peaks for Ile and Met residues located at, or near, the interface of the core and P1 domains in the crystal structure of SurA are the most broadened in the methyl-

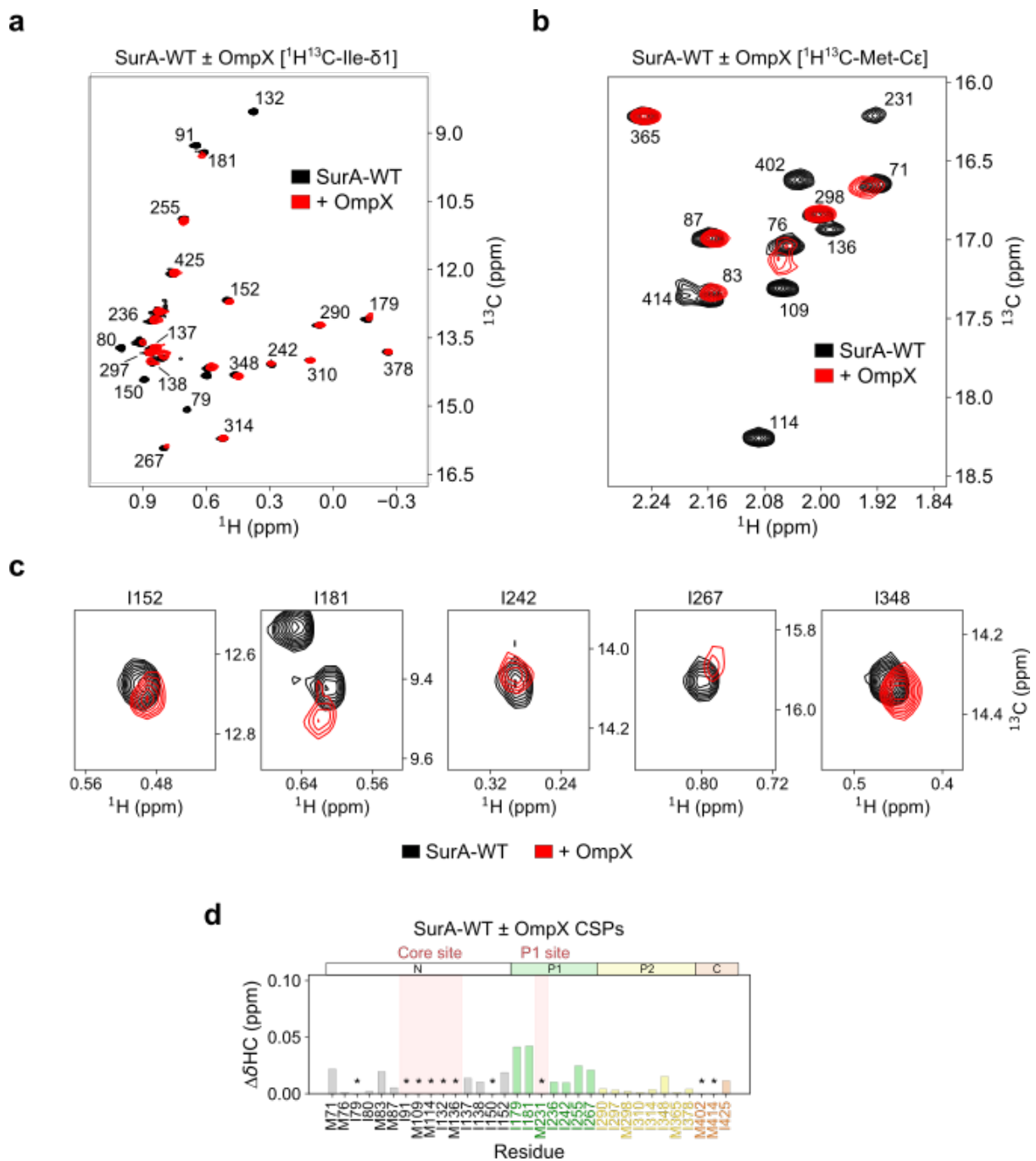
TROSY NMR spectrum of SurA-WT. **(a)** Locations of Ile and Met residues mapped onto the crystal structure of SurA (PDB: 1M5Y<sup>1</sup>). NMR-active <sup>13</sup>C-labelled atoms for Ile (C $\delta$ 1) and Met (C $\epsilon$ ) are highlighted as blue spheres. **(b)** Ile region, and **(c)** Met region of the NMR spectrum of apo-SurA (wild-type without client) with assignments. Two pairs of peaks are overlapped in the Ile spectrum (I70/I280) and (I100/I103). Peaks for I202/I259 and M46/M400 could not be unambiguously assigned (by mutating each residue individually (see Methods)). **(d,e)** Signal-to-noise ratios of peaks for **(d)** Ile and **(e)** Met in the NMR spectrum of apo-SurA. The most broadened peaks from residues in the core domain (M46, M400) and P1 domain (I217) are indicated by asterisks. Note that signal-to-noise ratios for peaks which are overlapped in the spectrum (corresponding to I70/I280 and I100/I103) could not be obtained and are omitted from **(d)**. **(f,g)** Two views of SurA highlighting residues in the core domain (M46, M400) and P1 domain (I217) whose corresponding peaks in the methyl-TROSY NMR spectrum of SurA-WT are the most broadened. Note that M46 is not directly in contact with the P1 domain (green) in the P1-closed conformation in the crystal structure, and additional dynamic movements within the core domain may contribute to its reduced relative intensity. Samples contained 5  $\mu$ M SurA, 5 mM, EDTA, 20 mM Tris-HCl, pH 8, at 25 °C. Source data are provided as a Source Data file.

**a**SurA-WT vs SurA- $\Delta$ P1 [ $^1\text{H}^{13}\text{C}$ -Ile-C $\delta$ 1]**b**SurA-WT vs SurA- $\Delta$ P1 [ $^1\text{H}^{13}\text{C}$ -Met-C $\epsilon$ ]**c**SurA-WT vs SurA- $\Delta$ P2 [ $^1\text{H}^{13}\text{C}$ -Ile-C $\delta$ 1]**d**SurA-WT vs SurA- $\Delta$ P2 [ $^1\text{H}^{13}\text{C}$ -Met-C $\epsilon$ ]**e**SurA-WT vs SurA-core [ $^1\text{H}^{13}\text{C}$ -Ile-C $\delta$ 1]**f**SurA-WT vs SurA-core [ $^1\text{H}^{13}\text{C}$ -Met-C $\epsilon$ ]

**Supplementary Fig. 4.** SurA domain deletion variants (**Fig. 1d**) suggest extensive interactions between SurA P1 domain and the core domain in SurA-WT. Methyl-TROSY NMR spectra of SurA-WT compared with (**a,b**) SurA- $\Delta$ P1, (**c,d**) SurA- $\Delta$ P2, and (**e,f**) SurA-core. Ile and Met regions are shown in (**a,c,e**) and (**b,d,f**), respectively. Spectra for SurA-WT, SurA- $\Delta$ P1, SurA- $\Delta$ P2, and SurA-core are coloured in black, magenta, red, and green, respectively. Two peaks for residues in the core domain (I70 and M400), which are highly broadened in the spectrum of SurA-WT, appear in the spectra for SurA variants lacking P1, and are highlighted in red font. Note the broadening of the peak for M414 which lies in SurA core in the spectra of all domain deletion variants. Samples contained 5  $\mu$ M SurA or SurA variant, 5 mM, EDTA, 20 mM Tris-HCl, pH 8, at 25 °C.

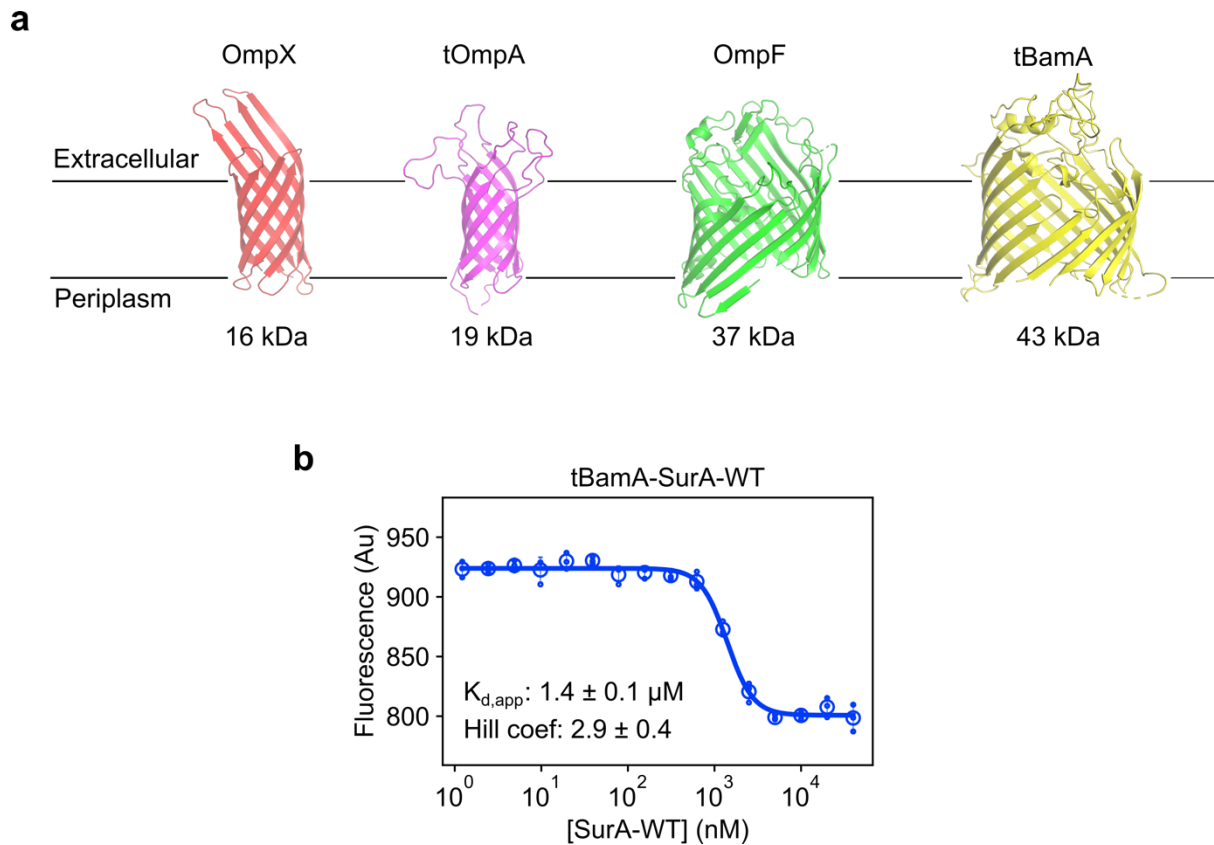


**Supplementary Fig. 5.** Chemical shift perturbations (CSPs) in the SurA core domain are greater in domain deletion variants lacking P1 (SurA- $\Delta$ P1 and SurA-core) compared with the P2 deletion construct (SurA- $\Delta$ P2). CSP plots are shown for (a) SurA- $\Delta$ P1 vs SurA-WT, (b) SurA- $\Delta$ P2 vs SurA-WT, and (c) SurA-core vs SurA-WT. Residue M414 in the core domain (red asterisk) is broadened in all variants. Residues which are not present in domain deletion constructs are indicated by black asterisks. Source data are provided as a Source Data file.

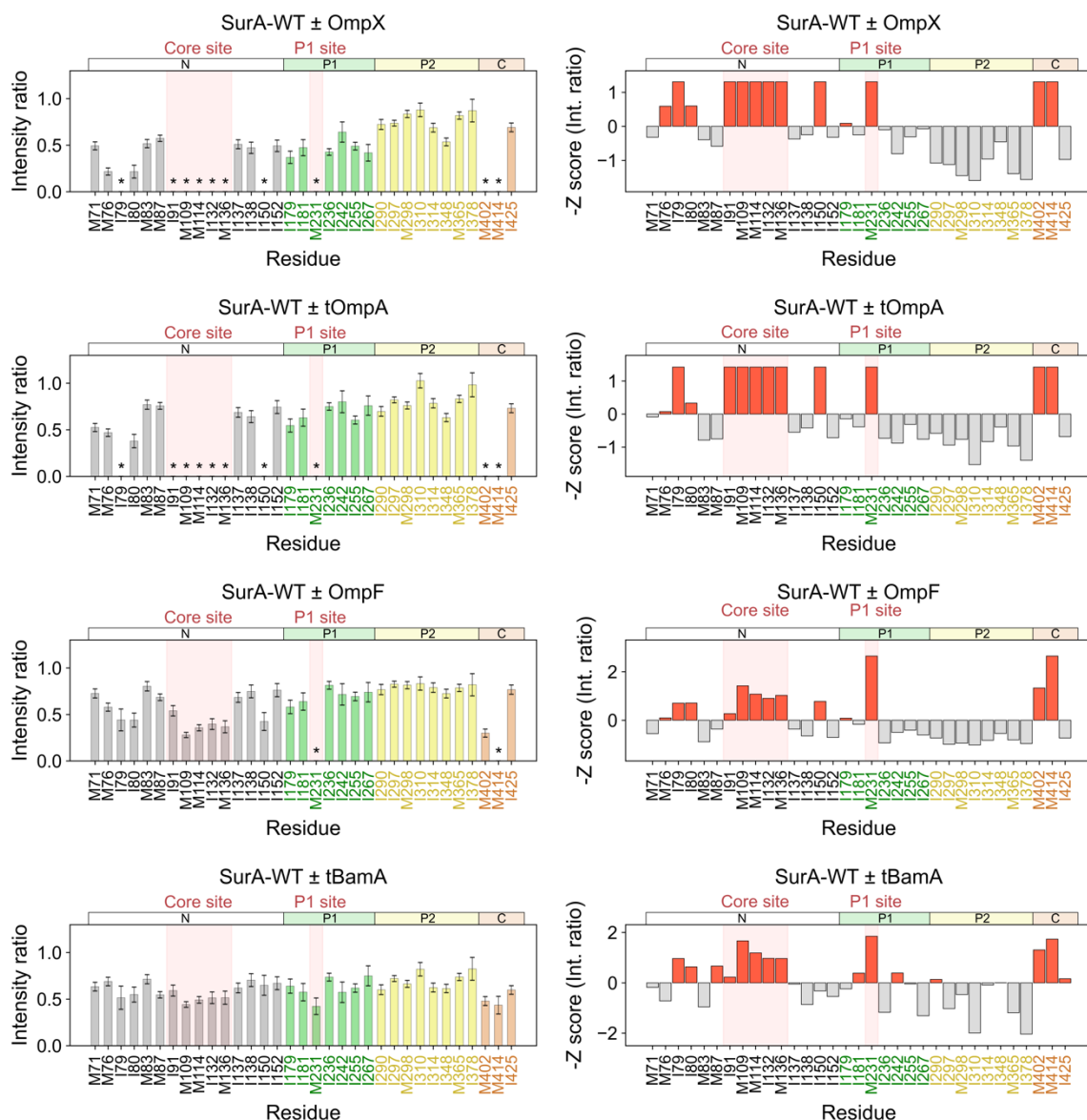


**Supplementary Fig. 6.** Interaction of SurA-WT with unfolded OmpX by methyl-TROSY NMR. (a,b) NMR spectra of SurA-WT alone (black) and with the addition of equimolar OmpX (red). Regions of the spectra containing (a) Ile peaks or (b) Met peaks are shown. (c) Zoomed in regions of spectra from (a) showing example CSPs in the P1 (I152, I181, I242, I267) and P2 (I348) domains. (d) CSPs for SurA-WT peaks in the presence of OmpX are shown, with residues broadened to below the noise indicated by an asterisk. Pink blocks indicate residues located in core and P1 binding hotspots, and are similarly highlighted in subsequent figures. Note that for apo-SurA-WT the broadened peaks for M400/M46 are not present in these

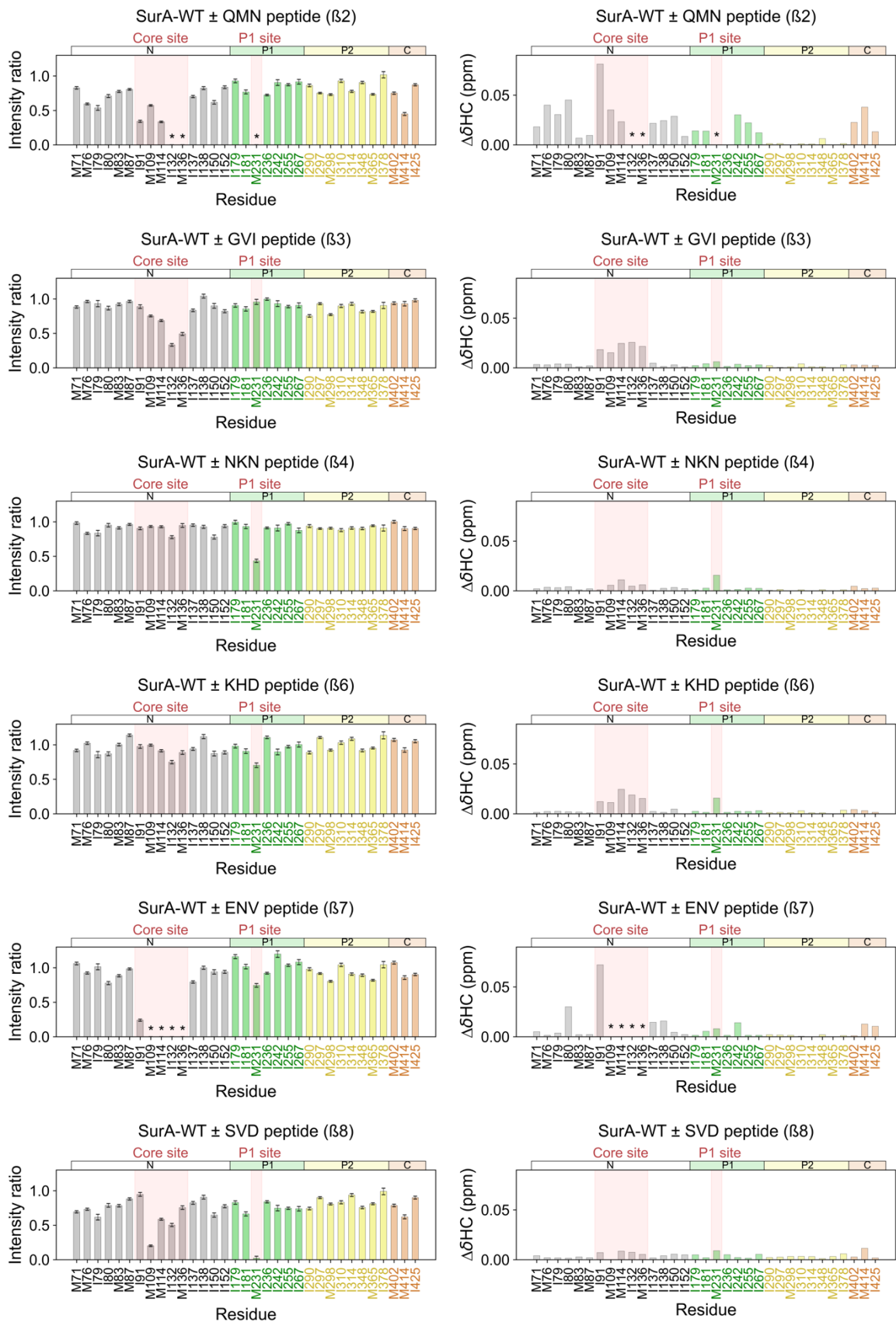
experiments in the presence of 0.8 M urea, and with shorter acquisitions compared to non-OMP containing experiments (see Methods). Samples contained 5  $\mu$ M SurA,  $\pm$  5  $\mu$ M OmpX, 0.8 M urea, 5 mM, EDTA, 20 mM Tris-HCl, pH 8, at 25 °C. Source data are provided as a Source Data file.



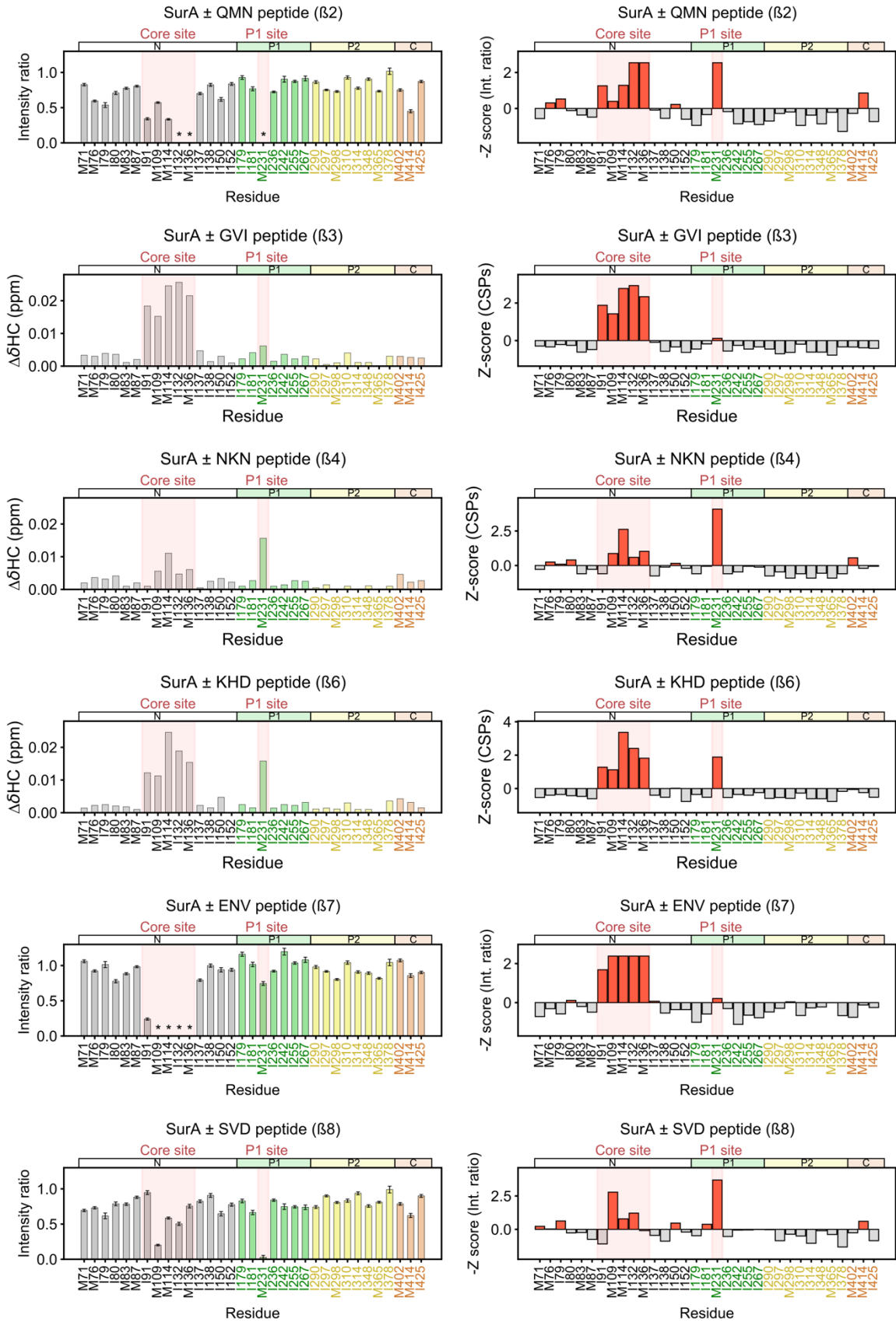
**Supplementary Fig. 7.** OMPs of different size and sequence used in this study. **(a)** Structures (from left to right) of natively folded OmpX (PDB: 1QJ8<sup>2</sup>), tOmpA (PDB: [1G90](#)<sup>3</sup>) OmpF (PDB: [2ZFG](#)<sup>4</sup>) and tBamA (PDB: [4N75](#)<sup>5</sup>). All OMPs are shown to scale. Note that OmpF is trimeric *in vivo*, a single subunit is shown here for direct size comparison. **(b)** Microscale thermophoresis (MST) data for binding of tBamA to SurA-WT. Samples contained 100 nM Alexa Fluor 488-labelled tBamA (Methods), SurA-WT (1.2 nM-40  $\mu\text{M}$ ), 20 mM Tris-HCl, pH 8, at 25 °C. Three independent replicates were performed and averaged prior to fitting. The mean for each SurA-WT concentration is shown as open circles and the individual values for each replicate are shown as dots. The error bars represent the standard deviation between replicates. Data were fitted to a Hill binding equation (see Methods). Source data are provided as a Source Data file.



**Supplementary Fig. 8.** OMPs of different size and sequence interact with similar locations on the surface of SurA. Changes in intensity ratios and the Z-scores of the intensity ratio changes are shown for SurA binding to unfolded OmpX, tOmpA, OmpF and tBamA. Each substrate was unfolded in 8M urea and diluted into SurA-WT to form the bound complex. Note that the absolute reductions in intensities are smaller for the larger OMPs, presumably because of differences in dynamics of the longer chains. Nonetheless, the locations affected are similar. Samples contained 5  $\mu$ M SurA,  $\pm$  5  $\mu$ M OMP, 0.8 M urea, 5 mM, EDTA, 20 mM Tris-HCl, pH 8, at 25  $^{\circ}$ C. Int: Intensity. Signal to noise ratios were used for the calculation of errors in peak intensities in intensity ratio panels (left) (Methods). Peaks which are broadened below the noise in the intensity ratio plots are indicated by an asterisk Source data are provided as a Source Data file.

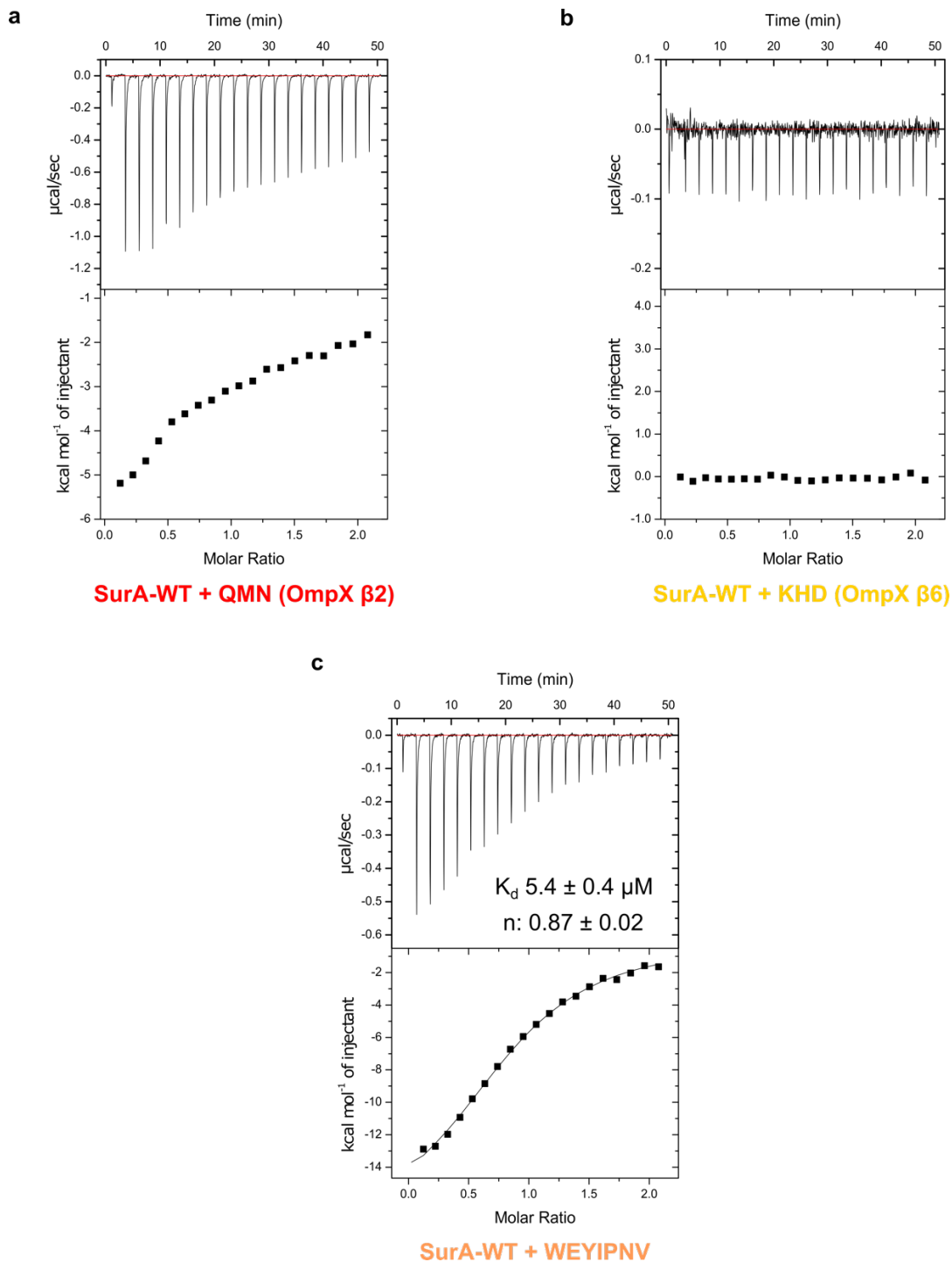


**Supplementary Fig. 9.** Intensity ratio and CSP data for SurA-WT binding to OmpX-derived peptides. Data are shown for peptide concentrations of 200  $\mu\text{M}$  except for the terminal  $\beta$ -strand peptide (SVD ( $\beta 8$ )), which was not soluble in NMR buffer at this concentration and therefore contained 50  $\mu\text{M}$  peptide. Each 15-residue peptide sequence corresponds to a different  $\beta$ -strand in the OmpX native state (**Fig. 3a,b**), with the strand number indicated in brackets. Samples contained 5  $\mu\text{M}$  SurA,  $\pm$  50 or 200  $\mu\text{M}$  OmpX-derived peptide (as detailed above), 0.8 M urea, 5 mM, EDTA, 20 mM Tris-HCl, pH 8, at 25  $^{\circ}\text{C}$ . Signal to noise ratios were used for the calculation of errors in peak intensities in intensity ratio panels (left) (Methods). Peaks which are broadened below the noise in the intensity ratio plots are indicated by an asterisk Source data are provided as a Source Data file.



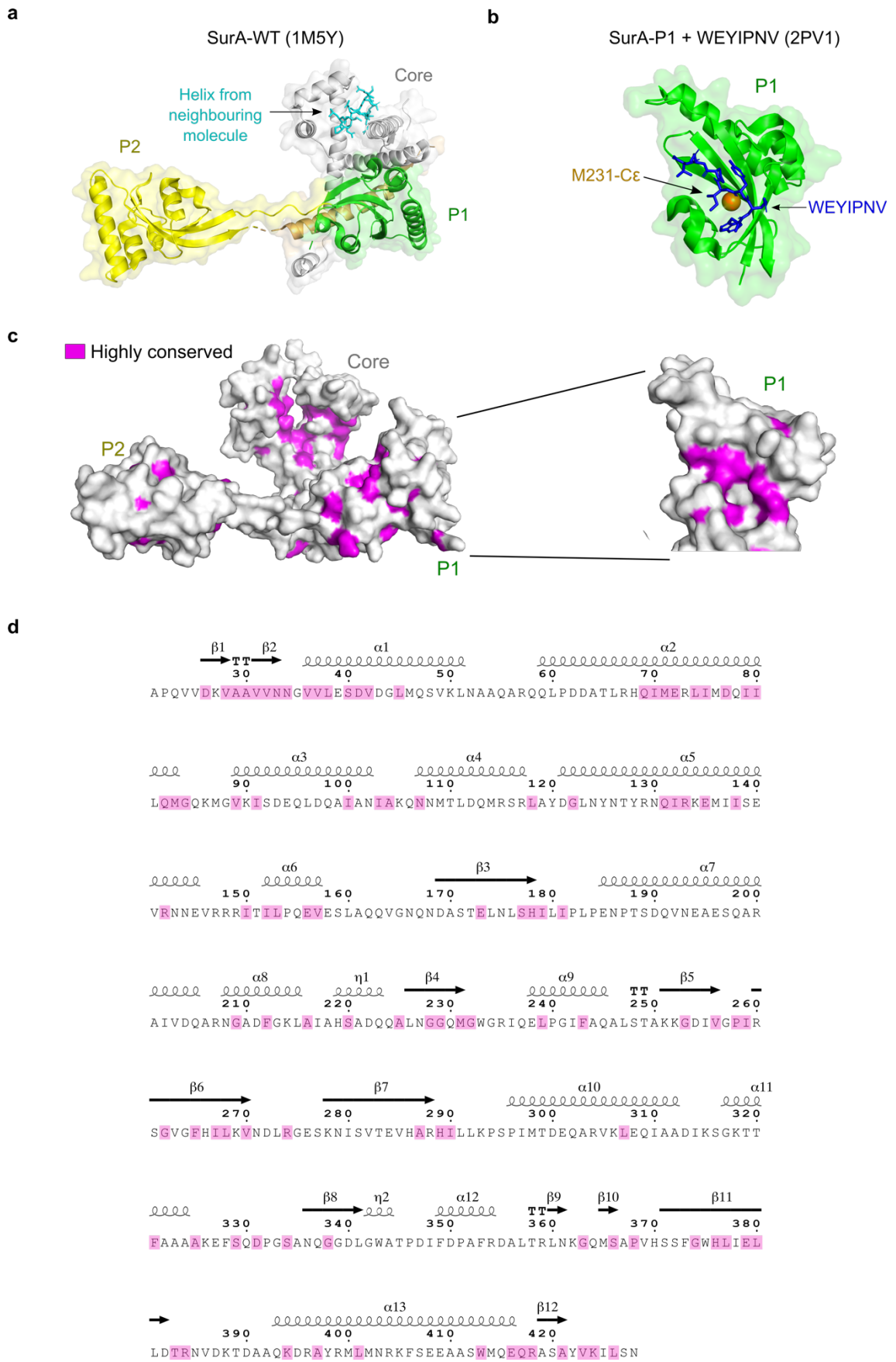
**Supplementary Fig. 10.** OmpX-derived peptides containing Ar-X-Ar or Ar-Ar motifs interact with two binding hotspots in the core and P1 domains of SurA-WT. Intensity ratio data are

shown for the QMN ( $\beta$ 2), ENV ( $\beta$ 7), and SVD ( $\beta$ 8) peptides. For the GVI ( $\beta$ 3), NKN ( $\beta$ 4) and KHD ( $\beta$ 6) peptides, the changes upon binding are mostly reflected in CSPs. Intensity ratio and CSP data for all peptides are shown in **Supplementary Fig. 9**. Peaks which are broadened below the noise in the intensity ratio plots are indicated by an asterisk. For these peaks, the noise value for the bound spectra were used in the calculation of Z-scores. Data are shown for peptide concentrations of 200  $\mu$ M, except for SVD ( $\beta$ 8), which contained 50  $\mu$ M due to its solubility limits. Each 15-residue peptide sequence corresponds to a different  $\beta$ -strand in the OmpX native state (**Fig. 3a,b**), with the strand number indicated in brackets. Samples contained 5  $\mu$ M SurA,  $\pm$  50 or 200  $\mu$ M OmpX-derived peptide (as detailed above), 0.8 M urea, 5 mM, EDTA, 20 mM Tris-HCl, pH 8, at 25 °C. Int: Intensity. Signal to noise ratios were used for the calculation of errors in peak intensities in intensity ratio panels (left) (Methods). Source data are provided as a Source Data file.



**Supplementary Fig. 11.** OmpX-derived peptides bind SurA-WT with weak affinity. ITC measurements for two example peptides **(a)** QMN ( $\beta$ 2) and **(b)** KHD ( $\beta$ 6). A full binding curve was not able to be obtained for any OmpX-derived peptide indicating weak affinities ( $>100 \mu\text{M}$ ). **(c)** For comparison, ITC data for binding of the WEYIPNV peptide to SurA-WT is shown, yielding an affinity consistent with literature values<sup>6</sup>. In **(a)** and **(b)** concentrations of  $100 \mu\text{M}$  SurA in the cell and  $1 \text{ mM}$  OmpX-derived peptides in the syringe were used. For **(c)**

concentrations of 20  $\mu\text{M}$  SurA in the cell and 200  $\mu\text{M}$  WEYIPNV peptide in the syringe were used. All samples contained 20 mM Tris-HCl, pH 8, and experiments were performed at 25  $^{\circ}\text{C}$ . Source data are provided as a Source Data file.



**Supplementary Fig. 12.** The two binding hotspots in SurA-WT contain highly conserved residues. **(a)** Crystal structure of SurA-WT (PDB: 1M5Y<sup>1</sup>) highlighting a short polypeptide sequence from a neighbouring molecule in the crystal structure (cyan) located in the core domain binding crevice. **(b)** Crystal structure of the WEYIPNV peptide (blue) bound to the SurA P1 domain (green) (PDB: 2PV1<sup>7</sup>). The location of the C $\epsilon$  atom of M231 is highlighted as an orange sphere. **(c)** Analysis of SurA three domain homologues (Methods) indicates high conservation for residues within the two binding sites identified here using NMR. Highly conserved residues (those with a ConSurf score of 7/9 or higher) are highlighted in magenta. The P1 domain alone is shown on the right, rotated to visualise residues in the binding pocket. Highly conserved residues in P2 are located in the catalytic site. **(d)** Primary sequence of SurA-WT with highly conserved residues highlighted in magenta as in **(c)**.

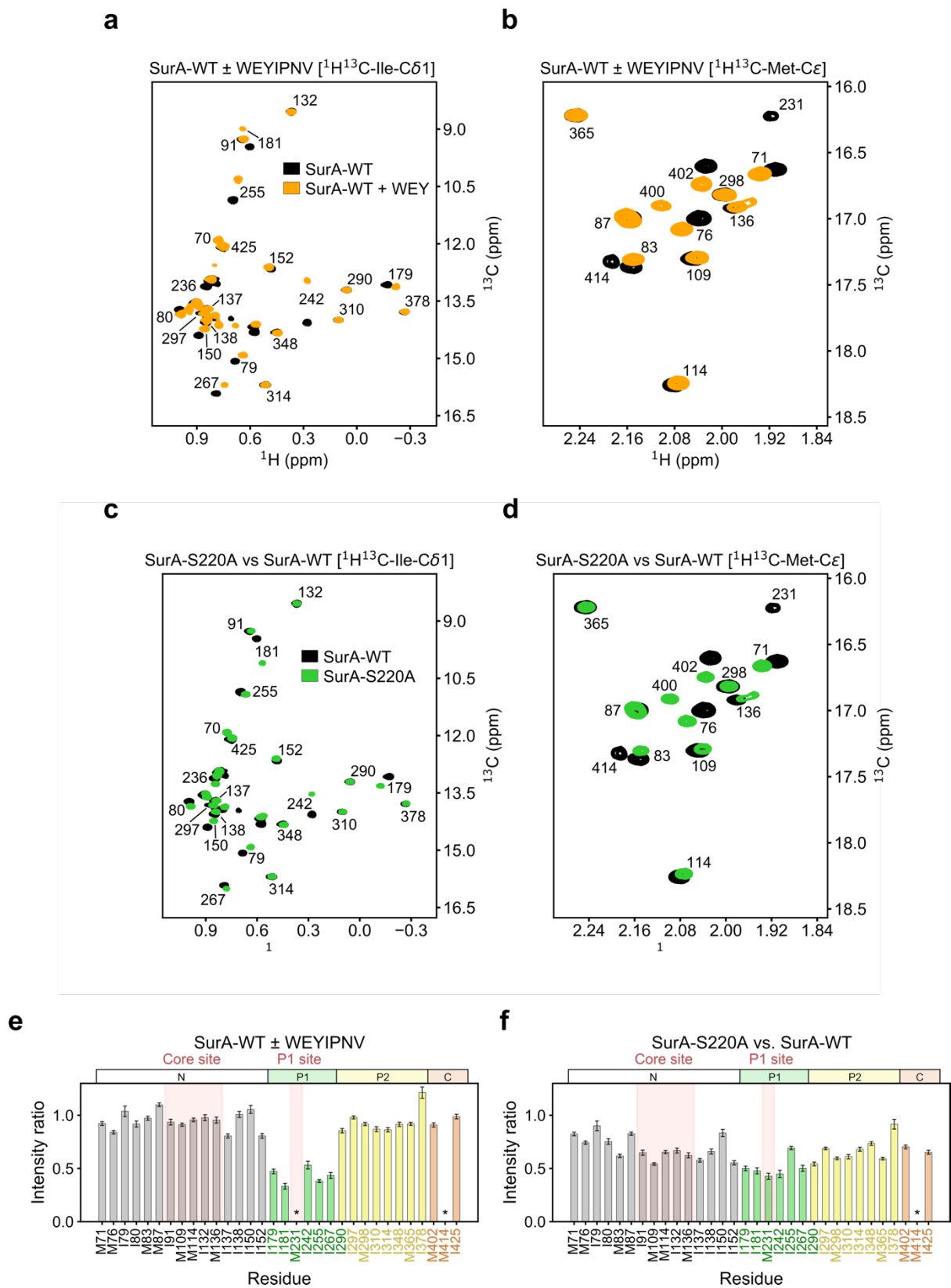
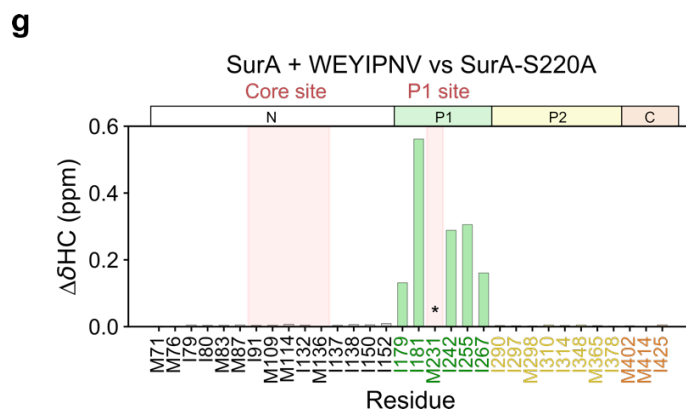
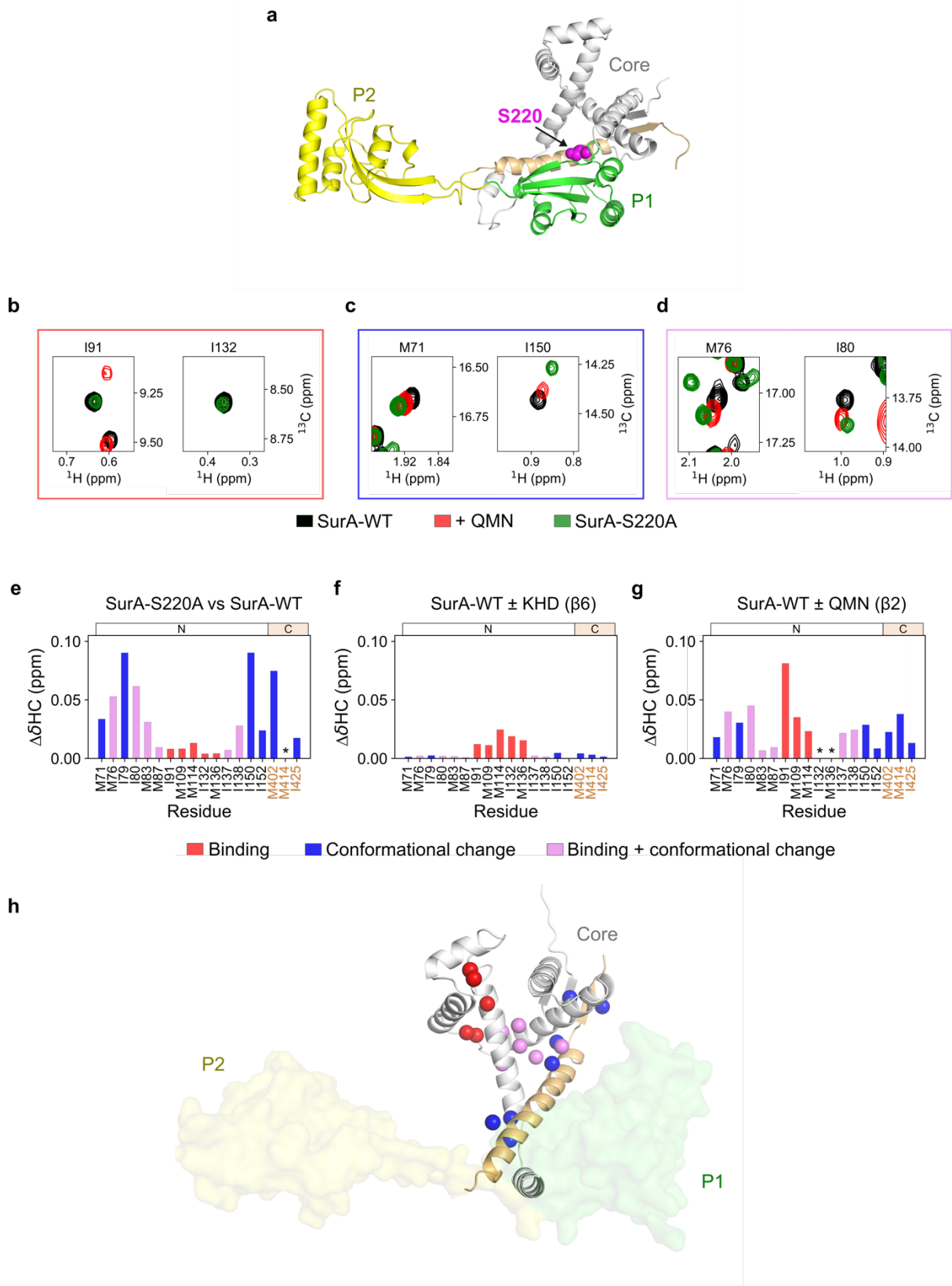


(Figure continued on next page)

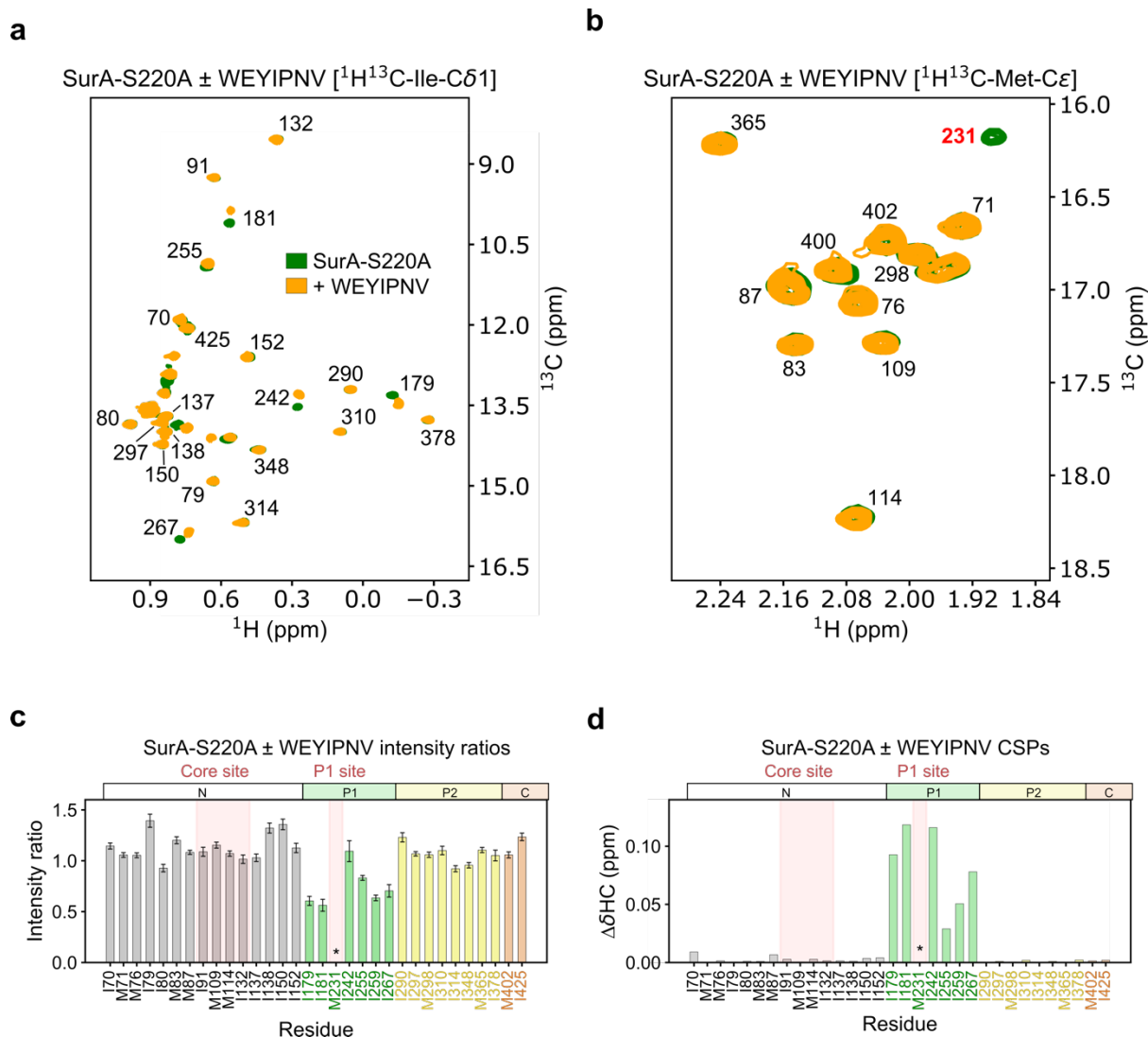


**Supplementary Fig. 13.** Binding of the WEYIPNV peptide to SurA-WT and the SurA-S220A variant cause similar conformational changes. Methyl-TROSY NMR spectra of (a,b) SurA-WT bound to WEYIPNV (orange) compared with SurA-WT alone (black) and (c,d) SurA-S220A (green) compared with SurA-WT alone (black). Ile and Met regions are shown in (a,c) and (b,d), respectively. (e,f) Intensity ratio changes between WEYIPNV-SurA-WT and SurA-WT, and SurA-S220A and SurA-WT, respectively. (g) Chemical shift differences between spectra of SurA-WT bound to WEYIPNV and SurA-WT vs. SurA-S220A, indicating similar chemical environments for core domain peaks in both cases. Resonances that have different chemical shifts in P1 are hence indicative of direct peptide binding. The peak corresponding to I236 in the spectrum of SurA-WT could not be confidently assigned for WEYIPNV-SurA-WT or SurA-S220A and so was excluded. Peaks which are broadened below the noise are indicated by an asterisk. Samples contained 5  $\mu$ M SurA-WT  $\pm$  50  $\mu$ M WEYIPNV or 5  $\mu$ M SurA-S220A, 5 mM EDTA, 20 mM Tris-HCl, pH 8, at 25  $^{\circ}$ C. Signal to noise ratios were used for the calculation of errors in peak intensities in (e) and (f) (Methods). Source data are provided as a Source Data file.

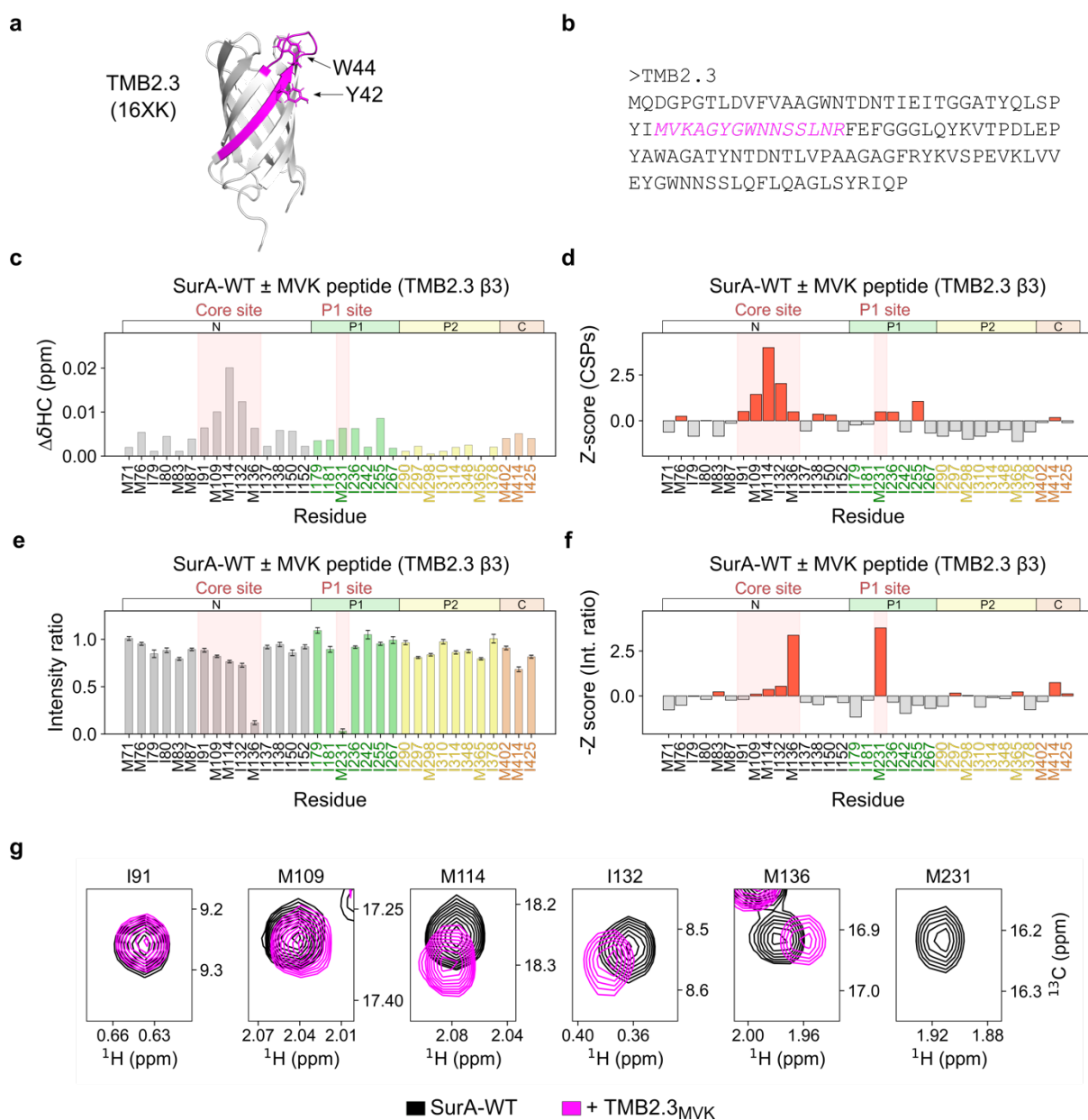


**Supplementary Fig. 14.** Binding of a peptide sequence derived from OmpX promotes a conformational rearrangement between the core and P1 domains to activate the chaperone.

(a) Residue S220 is located close to the core-P1 interface in the SurA core-P1 closed conformation (PDB: 1M5Y<sup>1</sup>). (b-d) Example zoomed in spectra comparing peaks in the spectra of SurA-WT alone, SurA-WT with the QMN ( $\beta$ 2) peptide (200  $\mu$ M), and SurA-S220A alone, which we classify as reporting mainly on (b) binding, (c) conformational changes, or (d) binding and conformational changes. Peaks were classified as reporting on conformational changes if the direction of the CSP upon binding of QMN to SurA-WT is identical to that between SurA-WT and SurA-S220A. Peaks were classified as reporting on binding and conformational changes if the CSP direction is similar, but not identical. (e-g) Zoom in on CSP plots showing core domain residues only for (e) SurA-S220A, (f) SurA-WT binding to the KHD ( $\beta$ 6) peptide (200  $\mu$ M), and (g) SurA-WT binding to the QMN ( $\beta$ 2) peptide (200  $\mu$ M). Bars are coloured by whether each peak reports largely on binding (red), conformational changes (blue), or binding and changes (violet), as judged by their behaviour in the NMR spectra. (h) Model of SurA in a core-P1 open conformation, highlighting which NMR probes in the core domain report on binding and/or conformational changes, coloured as in (f-h). Note that peaks which only report on conformational change (coloured blue) are located away from the binding site, and are close to the core-P1 interface. Peaks which are broadened below the noise are indicated by an asterisk. Source data are provided as a Source Data file.

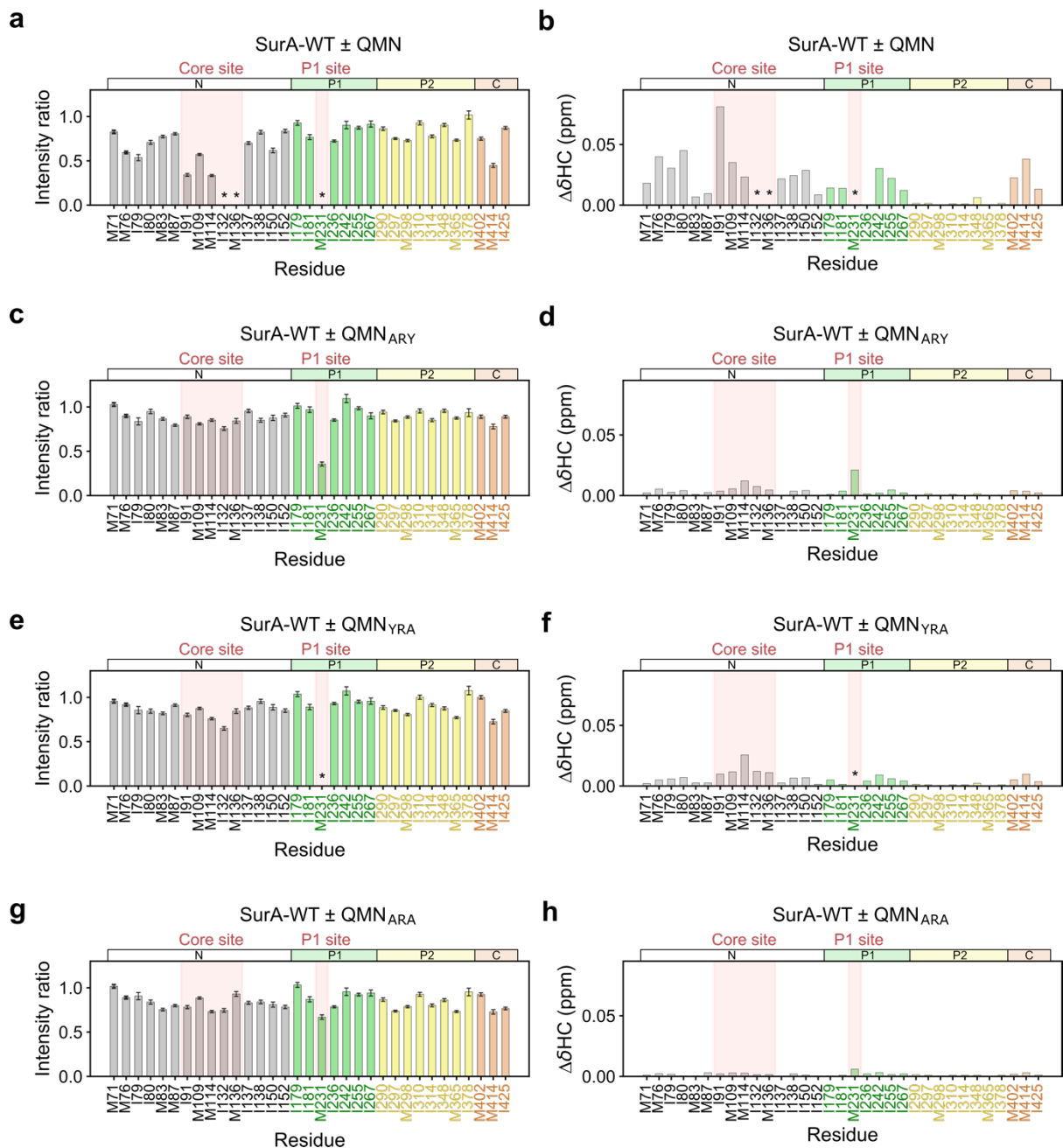


**Supplementary Fig. 15.** Loss of intensity of M231 peak in the methyl-TROSY NMR spectrum of SurA results from interaction with substrates. **(a,b)** Methyl-TROSY NMR spectra of SurA-S220A bound to WEYIPNV (orange) compared with SurA-S220A alone (green). Ile and Met regions are shown in **(a)** and **(b)**, respectively. The peak for M231 which is broadened in the presence of WEYIPNV is highlighted in red in **(b)** and highlighted with an asterisk in **(c)** and **(d)**. **(c)** Intensity ratios, and **(d)** CSPs between SurA-S220A alone and SurA-S220A bound to WEYIPNV. The peak corresponding to I236 in the spectrum of SurA-WT could not be confidently assigned for WEYIPNV-SurA-WT or SurA-S220A and so was excluded. The peak for M414 is broadened in the spectra of both WEYIPNV-SurA-WT and SurA-S220A so is not included in **(c)** and **(d)**. Samples contained 5  $\mu\text{M}$  SurA-S220A  $\pm$  50  $\mu\text{M}$  WEYIPNV, 5 mM EDTA, 20 mM Tris-HCl, pH 8, at 25  $^\circ\text{C}$ . Signal to noise ratios were used for the calculation of errors in peak intensities in **(c)** (Methods). Source data are provided as a Source Data file.



**Supplementary Fig. 16.** A peptide from the *de novo* designed transmembrane  $\beta$ -barrel TMB2.3<sup>8</sup> containing an Ar-X-Ar motif interacts with the identified OMP binding sites in the core and P1 domains of SurA. **(a)** Solution NMR structure of TMB2.3 (PDB: 16XK<sup>8</sup>). The 15-residue peptide beginning with the amino acids MVK (TMB2.3  $\beta$ 3) is highlighted in magenta on the structure. The aromatic residues of the Ar-X-Ar motif in this peptide (Y42 and W44) are indicated as sticks. **(b)** Primary sequence of TMB2.3 with the MVK peptide (TMB2.3  $\beta$ 3) highlighted in magenta. **(c)** CSPs and **(d)** Z-scores of the CSP data for the interaction between MVK (TMB2.3  $\beta$ 3) and SurA-WT. **(e)** Intensity ratios and **(f)** Z-scores of the intensity ratio data for the interaction of between MVK (TMB2.3  $\beta$ 3) and SurA-WT. **(g)** Zoomed in regions of NMR spectra for SurA alone (black), or SurA-WT in the presence of TMB2.3<sub>MVK</sub> (magenta)

highlighting regions of the spectra for residues indicative of interaction with the core (I91, M109, M114, I132, and M136), or P1 (M231) binding hotspots. Samples contained 5  $\mu$ M SurA  $\pm$  200  $\mu$ M TMB2.3<sub>MVK</sub>, 5 mM EDTA, 20 mM Tris-HCl, pH 8, at 25 °C. Signal to noise ratios were used for the calculation of errors in peak intensities in (e) (Methods). Source data are provided as a Source Data file.



**Supplementary Fig. 17.** Mutation of the Ar-X-Ar motif abolishes binding of an OmpX-derived peptide to SurA-WT. Intensity ratio (**a,c,e,g**) and CSP (**b,d,f,h**) plots are shown for SurA-WT bound to (**a,b**) peptide QMN ( $\beta$ 2) (QMNKMGGFNLKYRYE), (**c,d**) peptide QMN<sub>ARY</sub> (QMNKMGGFNLK<sup>ARY</sup>E), (**e,f**) peptide QMN<sub>YRA</sub> (QMNKMGGFNLKYR<sup>AE</sup>E) and (**g,h**) peptide QMN<sub>ARA</sub> (QMNKMGGFNLK<sup>ARAE</sup>E) (residues changed to Ala in red). Peaks which were broadened beyond detection in peptide-containing samples are indicated with an asterisk. Samples contained 5  $\mu$ M SurA  $\pm$  200  $\mu$ M peptide, 5 mM EDTA, 20 mM Tris-HCl, pH 8, at 25  $^{\circ}$ C. Signal to noise ratios were used for the calculation of errors in peak intensities in (a), (c), (e), and (g) (Methods). Peaks which are broadened below the noise are indicated by an asterisk. Source data are provided as a Source Data file.

	Repeat						Mean ( $\pm$ SD)
	1	2	3	4	5	6	
<b>OmpX N Labelled Alexa Fluor 488</b>	0.120	0.118	0.122	0.119	0.120	0.125	0.121 $\pm$ 0.002
<b>OmpX N Labelled ATTO 565</b>	0.082	0.066	0.087	0.100	0.088	0.108	0.080 $\pm$ 0.001
<b>OmpX C Labelled Alexa Fluor 488</b>	0.078	0.080	0.080	0.079	0.080	0.081	0.088 $\pm$ 0.015
<b>OmpX C Labelled ATTO 565</b>	0.076	0.082	0.076	0.086	0.084	0.085	0.081 $\pm$ 0.004

**Supplementary Table 1.** Steady state fluorescence anisotropy measurements. Single Cys variants of OmpX were labelled with either Alexa Fluor 488 or ATTO 565 on either the N- or C-termini and the fluorescence anisotropy measured (Supplementary Methods). The steady-state anisotropies of all the samples are similar and low, indicating good dye mobility, allowing changes in FRET efficiency to be attributed to changes in OmpX end-to-end distances.

Protein	$\beta$ -strand	Abbreviation	Residue numbers	Peptide
OmpX	$\beta$ 2	QMN	40-54	QMNKMGGFNLKYRYE
OmpX	$\beta$ 3	GVI	61-75	GVIGSFTYTEKSRTA
OmpX	$\beta$ 4	NKN	81-95	NKNQYYGITAGPAYR
OmpX	$\beta$ 6	KHD	122-136	KHDTSDYGFSGAGL
OmpX	$\beta$ 7	ENV	142-156	ENVALDFSYEQSRIR
OmpX	$\beta$ 8	SVD	157-172	SVDVGTWIAGVGYRF
Tmb2.3	$\beta$ 3	MVK	46-61	MVKAGYGWNNSSLNR
N/A	N/A	WEY	N/A	WEYIPNV
OmpX + mutation	$\beta$ 2	QMN-ARY	40-54	QMNKMGGFNLK <b>A</b> RYE
OmpX + mutation	$\beta$ 2	QMN-YRA	40-54	QMNKMGGFNLKYR <b>A</b> E
OmpX + mutation	$\beta$ 2	QMN-ARA	40-54	QMNKMGGFNLK <b>A</b> R <b>A</b> E
OmpX + mutation	$\beta$ 2	QMN-N-term	40-47	QMNKMGGF
OmpX + mutation	$\beta$ 3	QMN-C-term	48-54	NLKYRYE

**Supplementary Table 2.** Details of peptides used in this study. For the OmpX variants the residues changed are highlighted in red. The QMN N-term and C-term peptides are truncated at the C/N-termini, as indicated.

Core domain N-terminal mutants	P1 mutants	P2 mutants	Core domain C-terminal mutants
M46V	I179V	I280V	M400A
I70V	I181L	I290L	M402R
M71L	I202L	I297V	M414L
I75V	I217V	M298L	I425V
M76L	M231L	I310L	
I79L	I236L	I314L	
I80V	I242L	I348C	
M83L	I255V	M365L	
M87S	I259L	I378V	
I91V	I267L		
I100L			
I103V			
M109L			
M114L			
I132V			
M136L			
I137L			
I138L			
I150L			
I152V			

**Supplementary Table 3.** SurA isoleucine and methionine point mutants used in NMR peak assignment experiments. In each case the residue of interest was mutated to the most common substitution determined from a set of three domain SurA homologues curated from the PFAM database<sup>9</sup> and analysed using the ConsSurf server<sup>10</sup> (except for the I348C mutant).

<b>Protein</b>	<b>Extinction coefficient at 280 nm (M<sup>-1</sup> cm<sup>-1</sup>)</b>
SurA-WT	30,940
SurA-ΔP1	25,440
SurA-ΔP1	19,940
SurA-core	14,440
OmpX	34,840
tOmpA	46,870
OmpF	54,210
tBamA	101,315

**Supplementary Table 4.** Extinction coefficients at 280 nm used for determining protein concentration.

<b>Reagent</b>	<b>1 L</b>	<b>500 mL</b>	<b>250 mL</b>
Na <sub>2</sub> HPO <sub>4</sub> (anhydrous) (g)	13	6.5	3.25
KH <sub>2</sub> PO <sub>4</sub> (g)	6	3	1.5
NaCl (g)	1	0.5	0.25
<sup>15</sup> NH <sub>4</sub> Cl (g)	1	0.5	0.25
D-glucose (g)	2	1	0.5
Celtone Complete Medium (D) (mL)	10	5	2.5
MgSO <sub>4</sub> (anhydrous) (mg)	120	60	30
CaCl <sub>2</sub> (mg)	11	5.5	2.75
Biotin (mg)	10	5	2.5
Thiamine (mg)	10	5	2.5

**Supplementary Table 5.** Reagents used in NMR media for expression of deuterated, methyl-labelled SurA.

<b>Reagent</b>	<b>Code</b>
D <sub>2</sub> O	DLM-4-99-1000
D-glucose (1,2,3,4,5,6,6-D7, 98%)	DLM-2062-1
Celtone Complete Medium (D)	CGM-1040-D
$\alpha$ -ketobutyric acid (Ile labelling)	CDLM-7318
L-methionine (Met labelling)	CDLM-8885

**Supplementary Table 6.** Cambridge Isotopes Ltd (CIL) codes for reagents used in expression of deuterated, methyl-labelled SurA (Ile and Met residues).

## Supplementary Methods

### smFRET Instrumentation

smFRET experiments were performed on a custom-built confocal instrument using a Nikon Eclipse TE300 inverted microscope. Single molecules which diffused through the confocal volume were excited using PIE (pulsed interleaved excitation) with a 480 nm (PiL048XSM, Advanced Laser Diode Systems) and a 561 nm (PDL 800-D, PicoQuant) laser producing a total excitation frequency of 40 MHz<sup>11</sup>. The two laser beams were combined with a dichroic mirror (Di02-R561-25x36, Semrock) before being coupled into a single mode fibre (P3-460B-FC-1, Thorlabs Inc.) using an achromatic collimator (PAF2A-A15A, Thorlabs Inc.). The laser from the fibre was collimated (60FC-4-A11-01, Schäfer+Kirchhoff GmbH) and reflected from a dichroic mirror (Di03-R488/561-t1-25x36, Semrock) into a 60x 1.2 numerical aperture water immersion objective (UPLSAPO60XW, Olympus). Light emitted from the sample was recollected by the same objective before being focused by the tube lens through a 100 µm pinhole (P100D Thorlabs Inc.) and collimated (AC254-050-A, Thorlabs Inc.). The emission light is then split into two using a dichroic mirror (Di03-R561-t3-25x36, Semrock) before band-pass filters remove further excitation light in each channel (ET525/50m & ET605/52m, Chroma Technology GmbH). The two emission pathways are then focused by a lens (AC254-050-A, Thorlabs Inc.) onto two single-photon avalanche diodes (PD-100-CTD & PD-050-CTD, PicoQuant). Signal from the detectors and a sync signal from the laser was sent to a time-correlated single-photon counting data acquisition card (TimeHarp 260 PICO, PicoQuant). SymPhoTime64 software (PicoQuant) was used to acquire data.

### Fluorescence Anisotropy

Steady state fluorescence anisotropy was measured using a PTI QuantaMaster (Horiba Scientific). Prior to measurement samples were passed through a 30 kDa molecular weight cut off centrifugal filter to remove aggregates (Vivaspin 500, Sartorius). Samples were measured at 21 °C in a quartz glass cuvette (109004F-10-40, Hellma) at a volume of 1 ml and concentration of ~1 nM. The sample buffer was the same used for single-molecule FRET experiments without the antifading agent Trolox (20 mM Tris-HCl, 0.1 M urea, 0.02% (v/v) Tween-20, pH 8.0). For OmpX labelled with Alexa Fluor 488 the samples were excited at 495 nm and emission collected at 519 nm. For OmpX labelled with ATTO 565 the samples were excited at 564 nm and emission collected at 590 nm. The excitation and emission slits for all samples were set to 8 nm and 15 nm respectively. The grating correction factor was measured for each sample before the anisotropy measurement. Data acquisition and analysis were both performed using PTI FelixGX (v4.9.0.10243, Horiba Scientific).

## Supplementary References

1. Bitto, E. & McKay, D.B. Crystallographic structure of SurA, a molecular chaperone that facilitates folding of outer membrane porins. *Structure* **10**, 1489-98 (2002).
2. Vogt, J. & Schulz, G.E. The structure of the outer membrane protein OmpX from *Escherichia coli* reveals possible mechanisms of virulence. *Structure* **7**, 1301-9 (1999).
3. Arora, A., Abildgaard, F., Bushweller, J.H. & Tamm, L.K. Structure of outer membrane protein A transmembrane domain by NMR spectroscopy. *Nat Struct Biol* **8**, 334-338 (2001).
4. Yamashita, E., Zhalnina, M.V., Zakharov, S.D., Sharma, O. & Cramer, W.A. Crystal structures of the OmpF porin: function in a colicin translocon. *EMBO J* **27**, 2171-80 (2008).
5. Ni, D. et al. Structural and functional analysis of the  $\beta$ -barrel domain of BamA from *Escherichia coli*. *The FASEB Journal* **28**, 2677-2685 (2014).
6. Bitto, E. & McKay, D.B. The periplasmic molecular chaperone protein SurA binds a peptide motif that is characteristic of integral outer membrane proteins. *J Biol Chem* **278**, 49316-22 (2003).
7. Xu, X., Wang, S., Hu, Y.X. & McKay, D.B. The periplasmic bacterial molecular chaperone SurA adapts its structure to bind peptides in different conformations to assert a sequence preference for aromatic residues. *J Mol Biol* **373**, 367-81 (2007).
8. Vorobieva, A.A. et al. De novo design of transmembrane  $\beta$  barrels. *Science* **371**, eabc8182 (2021).
9. Humes, J.R. et al. The role of SurA PPIase domains in preventing aggregation of the outer-membrane proteins tOmpA and OmpT. *J Mol Biol* **431**, 1267-1283 (2019).
10. Ashkenazy, H. et al. ConSurf 2016: an improved methodology to estimate and visualize evolutionary conservation in macromolecules. *Nucleic Acids Res* **44**, W344-W350 (2016).
11. Müller, B.K., Zaychikov, E., Bräuchle, C. & Lamb, D.C. Pulsed interleaved excitation. *Biophys J* **89**, 3508-22 (2005).